Hindawi
Advances in Mathematical Physics
Volume 2017, Article ID 6894041, 13 pages
https://doi.org/10.1155/2017/6894041

Research Article

Robustness of Supercavitating Vehicles Based on Multistability Analysis

Yipin Lv, Tianhong Xiong, Wenjun Yi, and Jun Guan

National Key Laboratory of Transient Physics, Nanjing University of Science and Technology, Nanjing 210094, China

Correspondence should be addressed to Tianhong Xiong; xiongtianhong@njust.edu.cn

Received 23 January 2017; Accepted 9 March 2017; Published 5 April 2017

Academic Editor: Nikos Mastorakis

Supercavity can increase speed of underwater vehicles greatly. However, external interferences always lead to instability of vehicles. This paper focuses on robustness of supercavitating vehicles. Based on a 4-dimensional dynamic model, the existence of multistability is verified in supercavitating system through simulation, and the robustness of vehicles varying with parameters is analyzed by basins of attraction. Results of the research disclose that the supercavitating system has three stable states in some regions of parameters space, namely, stable, periodic, and chaotic states, while in other regions it has various multistability, such as coexistence of two types of stable equilibrium points, coexistence of a limit cycle with a chaotic attractor, and coexistence of 1-periodic cycle with 2-periodic cycle. Provided that cavitation number varies within a small range, with increase of the feedback control gain of fin deflection angle, size of basin of attraction becomes smaller and robustness of the system becomes weaker. In practical application, robustness of supercavitating vehicles can be improved by setting parameters of system or adjusting initial launching conditions.

1. Introduction

When vehicle navigates underwater at a high speed, water pressure on surface of supercavitating vehicle will decrease. Once the speed is increased to a critical value, pressure of water will reach the level of vaporization; then the water will change from liquid phase to vapor phase, which is called cavitation [1]. With unceasing increase of speed, as shown in Figure 1, the cavity will move backward and expand along the surface of vehicle and finally develops into supercavity [2, 3] which envelops the whole vehicle. Different conditions of flow field and geometric shapes of vehicles lead to various typical states of supercavity almost completely. In study of cavitating flow, a dimensionless parameter σ is often used to characterize the extent of cavitation, namely, cavitation number, defined as $\sigma = 2(p_\infty - p_c)/\rho V^2$, where ρ is the density of water, p_∞ is the ambient pressure at infinity, p_c is the cavity pressure, and V refers to the velocity of vehicle [4]. After formation of supercavity, the resistance of water turns into the resistance of cavity consisting of vapor, which increases the velocity greatly and enables supercavitating vehicle to "fly" underwater. Despite remarkable reduction of resistance by supercavity, supercavitating vehicle in high speed will be covered by supercavity substantially or wholly, which results in decrease of wetting area, loss of most buoyancy, and forward drift of pressure center, decrease of attached quality, and damping torque accordingly. All these factors make supercavitating vehicle sensitive to ambient interferences; robustness of supercavitating vehicle is thus weakened [5, 6]. In addition, change in fin deflection angle always affects attitude of vehicle inside supercavity. Change in cavitation number also affects the size of supercavity, which leads to collision between tail of vehicle and supercavity, and results in the generation of nonlinear planning force. Nonlinear planning force brings not only greater friction to supercavitating vehicle, but also vibration and shock, as well as complex nonlinear physical phenomena, such as bifurcation and chaos, which poses a challenge to dynamic modeling, guidance, and control [7, 8]. Therefore, efficient control on attitude of supercavitating vehicle inside supercavity, improvement of robustness of motion, and reduction of shock from collision between supercavitating vehicle and supercavity are critical

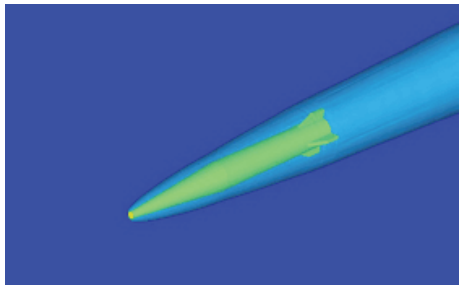

Figure 1: Illustration of vehicle inside supercavity.

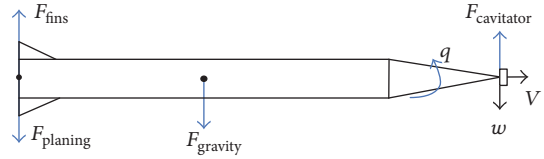

Figure 2: Structure and forces of supercavitating vehicle.

to ensure the stable motion of underwater supercavitating vehicle.

Unique navigation environment of supercavitating vehicle has predetermined that it is a multivariable system with complex couplings and uncertain hydrodynamic parameters. Supercavitating vehicle is different from common underwater vehicle; both particularities of control object such as nonlinearity of the planning force and uncertainty of supercavitating vehicle as well as the robustness with external interferences should be taken into consideration. There are a few papers published regarding the study of robustness. Linear state-feedback control method, presented by Lin et al. [9], achieved strong robustness in error of modeling for planning force of supercavitating vehicle. Vanek and Balas [10] considered uncertainty in shape of supercavity, and the control with linear parameter variables ("LPV") after linearization of feedback was researched. Goel [11] applied robustness control to the design and analysis of linear model of supercavitating vehicle with target to uncertainty of its hydrodynamic parameters. Zhao et al. [12] considered the uncertainty (existing in linear model of supercavitating vehicle) and unmodeled dynamics (mainly displayed by hydrodynamic coefficient perturbation in simulation) and applied robustness control to the design of controller. Wang and Zhao [13] applied principle of minor perturbation to linearization of longitudinal motion model of supercavitating vehicle, and control methods were further researched based on linear feedback theory and robustness control theory. Although some achievements have been made on the uncertainty existing in hydrodynamic model of supercavitating vehicle and external perturbation in above researches, it is inevitable to ignore many nonlinear factors in the process of linearization which brings some limitations to actual application, and the particularity of control object, namely, supercavitating vehicle, cannot be described accurately due to error of modeling. In the current work, the robustness of supercavitating vehicle is studied with nonlinear planning force taken into consideration.

On the other hand, the studies on multistability analysis are mainly made on phase-locked-loop circuits models [14, 15], electrical machines models [16, 17], and aircraft models [18, 19], to disclose causes why the systems are susceptible to intrinsic parameters, which is helpful to improve efficiency of transformations in circuits and prevent aircraft from crashing, with great significance to stability design and utilization of chaos. However, the above nonlinear models are all low-dimensional, while the model of supercavitating vehicle is different from others, which is 4-dimensional in this paper. Furthermore, aircrafts move only in the air, while underwater supercavitating vehicles move at high speed inside supercavity. The liquid-vapor interface between supercavity and water flows instability, resulting in complicated cavity dynamics; the nonlinear forces that the vehicle experiences are stronger than aircraft. Due to the complexity of underwater environment, the motion stability is affected by more system parameters, which are coupled and constrained with each other, increasing the complexity of the model, so it always leads to unexpected motion; the system dynamics presents challenges to stabilization and the motion robustness of the body. In order to solve this problem, it is necessary to make a thorough study on unpredictable factors of the system to prevent unexpected damage. Therefore, it is significance to study the motion stability through multistability analysis.

In the paper, various coexisting attractors can be found by adjusting initial values of the system based on a 4-dimensional nonlinear hydrodynamic model of supercavitating vehicle, after systematic parameters are determined. Seen from angle of engineering, estimation of basins of attraction enables us to know which perturbations are acceptable to the system and which (leading to instability of supercavitating vehicle) are not. On such basis, the relation between robustness of vehicle and the size and change of basins of attraction can be analyzed further, which provides parameters and initial values for launching stable supercavitating vehicle, as well as necessary base of research for the design of controller of supercavitating vehicle.

2. Dynamic Description of Underwater Supercavitating Vehicle

The structure and forces of supercavitating vehicle are shown in Figure 2, supercavitating vehicle is a rotating body, the head is cavitator, the forepart is a frustum, the middle part is a column, and the tail is a stretching apron-like fin. When the vehicle is fully contained in the cavity, the only hydrodynamic forces acting are due to the cavitator and immersed fins. Main forces exerted on supercavitating vehicle are the lift on the cavitator $F_{cavitator}$, the lift on the fin F_{fins}, the gravity in the center of supercavitating vehicle $F_{gravity}$, and the nonlinear planning force $F_{planing}$.

The lift on the cavitator is approximately [4]

$$F_{cavitator} = \frac{1}{2}\pi\rho R_n^2 V^2 C_x \alpha_c. \quad (1)$$

In the above equation, C_x denotes the cavitator drag coefficient and $C_x = C_{x0}(1+\sigma)$, where $C_{x0} = 0.82$. α_c denotes the angle of attack due to cavitator deflection δ_c and vertical velocity V. Similarly, the lift on the fin is approximately [4]

$$F_{\text{fin}} = -n\frac{1}{2}\pi\rho R_n^2 V^2 C_x \alpha_f. \tag{2}$$

In (2), the parameter n represents the efficiency of the fin, which is the ratio of the length of the fin immersed in the water to the total length of the fin and α_f denotes the angle of attack due to fin deflection δ_f and vertical velocity V.

When the vehicle body navigates in supercavity, due to the change of relative position of the body and the cavity, the tail and the cavity will touch with each other which will produce a complex nonlinear planning force, resulting in vibration and shock; the normalized force F_{planing} is [4]

$$F_{\text{planing}} = -V^2\left[1 - \left(\frac{R'}{hR + R'}\right)^2\right]\left(\frac{1+h}{1+2h}\right)\alpha. \tag{3}$$

In the previous equation, $R' = R_c - R$, R_c denotes the radius of the cavity, and R denotes radius of vehicle. The immersion depth h and the angle of attack α in the planning force are given by [4]

$$h = \begin{cases} 0 & |w| < w_{\text{th}} = \dfrac{(R_c - R)V}{L} \\ \dfrac{L|w|}{RV} - \dfrac{R_c - R}{R} & \text{otherwise,} \end{cases}$$
$$\alpha = \begin{cases} \dfrac{w - \dot{R}_c}{V} & \dfrac{w}{V} > 0 \\ \dfrac{w + \dot{R}_c}{V} & \text{otherwise.} \end{cases} \tag{4}$$

In (4), w is the vertical velocity, L is the vehicle length, and $\dot{R}_c$ is the cavity radius contraction rate.

Dzielski and Kurdila [4] presented a simplified 4-dimensional dynamic model of supercavitating vehicle. Although only the effect of angle of attack on planning force is considered in the model, motion characteristics of supercavitating vehicle in vertical plane can be described qualitatively. Following the work of Dzielski and Kurdila, in present work, a dynamic model of supercavitating vehicle is established by two bifurcation parameters.

The center of top surface of the disk-shaped cavitator on head of supercavitating vehicle is taken as the origin of coordinate system. The four state variables are used to describe dynamic of supercavitating vehicle in the model, namely, z, w, θ, and q, wherein z represents the depth where the body is located, w is the vertical velocity, and θ and q refer to the pitch and pitch rate, respectively. The vertical velocity w is perpendicular to the axial line of supercavitating vehicle, and forward velocity V is parallel to the axial line. In addition, the system has two control inputs, namely, cavitator deflection angle δ_c and fin deflection angle δ_e. In the classic control law presented by Dzielski and Kurdila [4], $\delta_e = 0$ and $\delta_c = 15z\text{-}30\theta\text{-}0.3q$. However, supercavitating vehicle would lack supportive force of fin due to $\delta_e = 0$. If the lift on the cavitator $F_{\text{cavitator}}$ could not overcome the weight of supercavitating vehicle, vehicle would immerse into supercavity result in unstable motion. Therefore, the control law in the paper is chosen as $\delta_e = -kz$, $\delta_{c1} = 15z\text{-}30\theta\text{-}0.3q$, in which k refers to the feedback control gain of z. According to fluid dynamics exerted on different parts of supercavitating vehicle, the dynamic model [7] can be established with cavitation number σ and feedback control gain of fin deflection angle k as variable parameters:

$$\begin{pmatrix} \dot{z} \\ \dot{w} \\ \dot{\theta} \\ \dot{q} \end{pmatrix} = \begin{pmatrix} 0 & 1 & -V & 0 \\ 0 & a_{22} & 0 & a_{24} \\ 0 & 0 & 0 & 1 \\ 0 & a_{42} & 0 & a_{44} \end{pmatrix}\begin{pmatrix} z \\ w \\ \theta \\ q \end{pmatrix} + \begin{pmatrix} 0 & 0 \\ b_{21} & b_{22} \\ 0 & 0 \\ b_{41} & b_{42} \end{pmatrix}\begin{pmatrix} \delta_e \\ \delta_c \end{pmatrix} + \begin{pmatrix} 0 \\ c_2 \\ 0 \\ 0 \end{pmatrix} + \begin{pmatrix} 0 \\ d_2 \\ 0 \\ d_4 \end{pmatrix} F_{\text{planing}}. \tag{5}$$

In (5),

$$a_{22} = \frac{CVT}{m}\left(\frac{-1-n}{L}\right)S + \frac{17}{36}nL,$$
$$a_{24} = VTS\left(C\frac{-n}{m} + \frac{7}{9}\right) - VT\left(C\frac{-n}{m} + \frac{17}{36}\right)\frac{17}{36}L^2,$$
$$a_{42} = \frac{CVT}{m}\left(\frac{17}{36} - \frac{11n}{36}\right),$$
$$a_{44} = \frac{-11CVTnL}{36m},$$
$$b_{21} = \frac{CV^2Tn}{m}\left(\frac{-S}{L} + \frac{17L}{36}\right),$$
$$b_{22} = \frac{-CV^2TS}{mL},$$
$$b_{41} = \frac{-11CV^2Tn}{36m},$$
$$b_{42} = \frac{17CV^2T}{36m},$$
$$c_2 = g,$$
$$d_2 = \frac{T}{m}\left(\frac{-17L}{36} + \frac{S}{L}\right),$$

Table 1: Parameters of supercavitating vehicle model.

Parameter	Description	Value
g	Acceleration of gravity	9.81 m/s^2
m	Density ratio (ρ_m/ρ)	2
n	Tail efficiency	0.5
R_n	Radius of cavitator	0.0191 m
R	Radius of vehicle	0.0508 m
L	Length of vehicle	1.8 m
σ	Cavitation number	[0.01980, 0.03680]
C_{x0}	Coefficient of lift	0.82

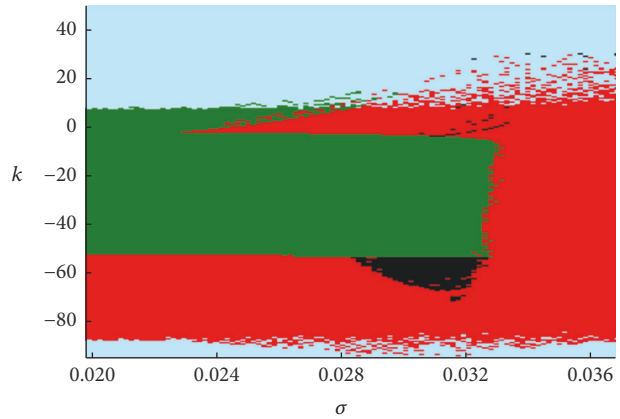

Figure 3: Distribution diagram of dynamic behaviors of supercavitating vehicle.

$$d_4 = \frac{11T}{36m},$$
$$S = \frac{11}{60}R^2 + \frac{133L^2}{405},$$
$$T = \frac{1}{7S/9 - 289L^2/1296},$$
$$C = 0.5C_{x0}(1+\sigma)\left(\frac{R_n}{R}\right)^2. \quad (6)$$

m (ρ_m/ρ) denotes density ratio, where ρ_m is the specification of a uniform density for the vehicle and ρ is the density of water.

3. General Dynamic Characteristics of Supercavitating Vehicle

Values of parameters for supercavitating vehicle model are given in Table 1 [7]. Based on dynamic model (5), the initial conditions are selected randomly. According to the Lyapunov stability theory, the stable solutions, periodic solutions, and chaotic solutions of the model are represented by green, red, and black in Figure 3, respectively. The distribution diagram of dynamic behaviors, defined by cavitation number σ and feedback control gain of fin deflection angle k as the bifurcation parameters, is drawn. And the dependence of dynamic behaviors on σ and k is described. As shown in Figure 3, if value of σ, k is within the green region, the max Lyapunov exponent of (5) is a negative, and state variables z, w, θ, and q converge on stable equilibrium points; supercavitating vehicle can move steadily. If the point (σ, k) is within the red region, the max Lyapunov exponent of (5) is zero, and state variables z, w, θ, and q oscillate periodically centering on stable equilibrium points, therefore, supercavitating vehicle shock periodically. If (σ, k) is within the black region, the max Lyapunov exponent of (5) is a positive, and state variables z, w, θ, and q oscillate violently and irregularly, violent vibrations and shocks will occur, and then supercavitating vehicle will capsize. The light blue region represents where the system is divergent and vehicle cannot navigate.

Figure 3 reflects different dynamics of supercavitating vehicle completely when the parameters σ and k change simultaneously. The range of parameters corresponding to stable motion of vehicle can be determined by the dynamic distribution diagram. When cavitation number σ is constant, the value of feedback control gain of fin deflection angle k can be adjusted within the green stable region and the red periodic region to realize stable motion of supercavitating vehicle efficiently, which is instructive to stability control of supercavitating vehicle. It can be seen from Figure 3 that one has the following:

(1) The horizontal section is bifurcation diagram of the system varying with σ, while the vertical section is bifurcation diagram of the system varying with k. The bifurcation diagram reflects the rules of changes of the system with parameters and complex nonlinear physical phenomena generated. The Hopf bifurcation always occurs when the system switches from steady state to periodic state, so the boundary between the red region and the green region in Figure 3 is critical line between steady state and periodic state, also called the Hopf bifurcation line. The boundary between the red region and the black region represents the switching between the periodic state and the chaotic state. There are nonlinear physical phenomena, such as the cutting bifurcation or period-doubling bifurcation at this boundary.

(2) Supercavitating vehicle has three stable states, including stable motion, periodic motion, and chaotic state. Select one point from the three regions, respectively; the projections of phase tracks on w-θ plane are shown in Figure 4. Select $\sigma = 0.02249$, $k = -14.05$ from the green region, as shown in Figure 4(a); vertical velocity w and pitch θ are attracted to a stable equilibrium point functioned by feedback control law; supercavitating vehicle is exerted by forces in equilibrium state, navigating stably in fixed position, and attitude inside supercavity, with oblique small angle of attack. Select $\sigma = 0.03459$, $k = -1.75$ randomly from the red region, as shown in Figure 4(b), mapping of the system forms a closed limit cycle, and the limit cycle intersects the red switching critical line

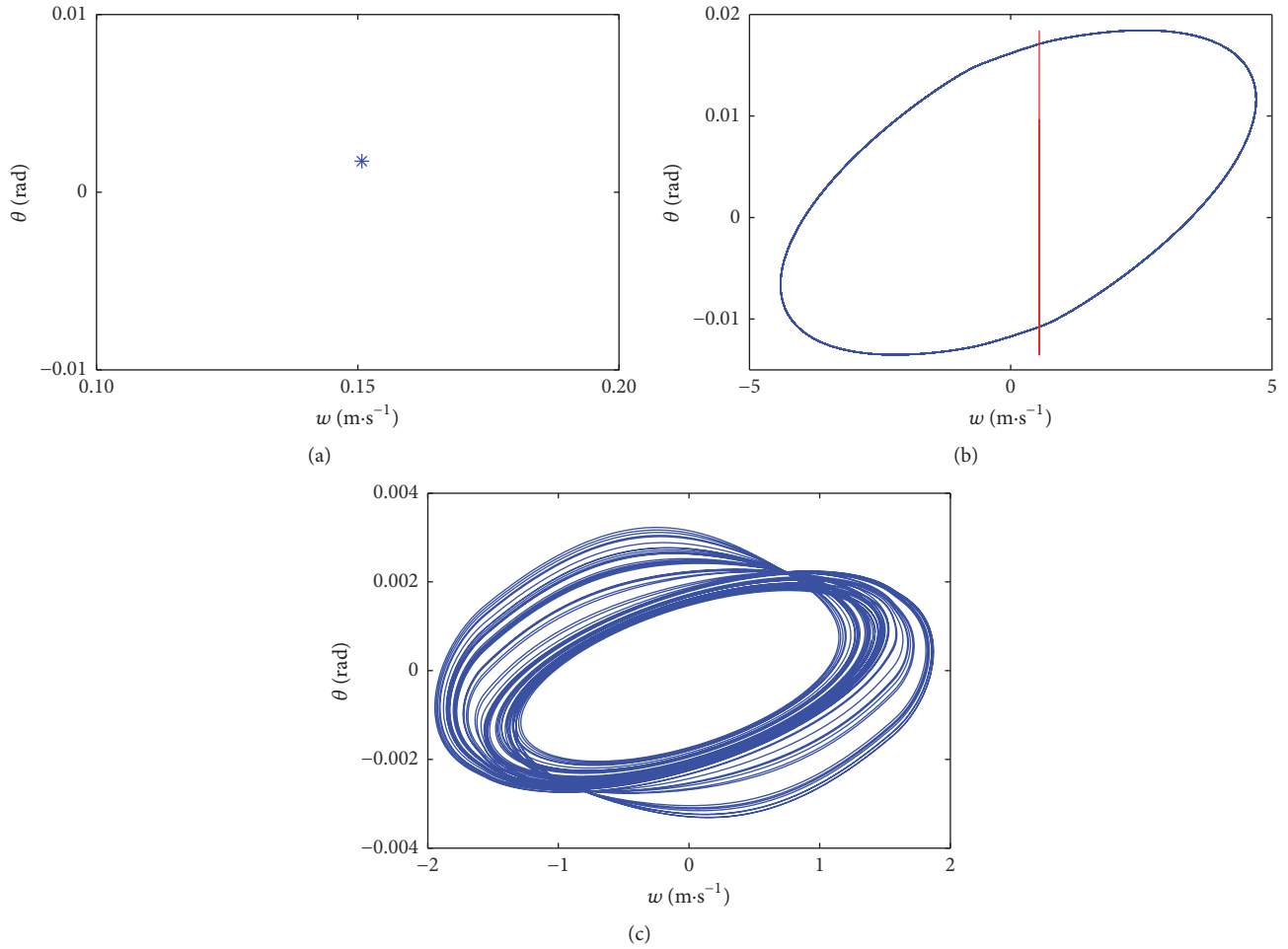

FIGURE 4: Phase tracks of three stable states on w-θ plane: (a) $\sigma = 0.02249$, $k = -14.05$; (b) $\sigma = 0.03459$, $k = -1.75$; (c) $\sigma = 0.03040$, $k = -59.13$.

$w = w_{\text{th}}$, where, $w_{\text{th}} = (Rc - R)V/L$ [7], Rc is the radius of supercavity, and vertical velocity w fluctuates around w_{th}. Tail of supercavitating vehicle oscillates from time to time touching the supercavity, which leads to periodic change of planning force, sometimes the tail penetrates the supercavity and inserts into water to generate planning force, and sometimes it is enclosed by the supercavity and thus no planning force is generated, and supercavitating vehicle oscillates periodically. Select parameters $\sigma = 0.03040$, $k = -59.13$ randomly from the red region; appearance of chaotic attractor indicates that supercavitating vehicle has complex nonlinear dynamic behavior and is likely to capsize. In practical application of engineering, effective control should be taken to prevent occurrence of such circumstance.

(3) Within $\sigma \in [0.0262, 0.02973]$, $k \in [7.387, 14.32]$, the green stable region, the red periodic region, and the divergent region are interwoven; stable equilibrium points coexist with periodic attractors in the region. When $\sigma = 0.02771$, $k = 7.883$, if initial values are $(z_0, w_0, \theta_0, q_0) = (0.49, 1.03, 0.73, -0.31)$, the phase track converges to a stable equilibrium point. If initial values are $(z_0, w_0, \theta_0, q_0) = (0.29, -0.79, 0.89, -1.15)$, the phase track is a limit cycle. Projections of the coexisting attractor in two-dimensional plane w-θ and three-dimensional space w-θ-q are shown in Figures 5(a) and 5(b), respectively, in which the red dot represents equilibrium point attractor and the blue limit cycle represents periodic attractor. Within $\sigma \in [0.02745, 0.03255]$, $k \in [-76.85, -52.57]$, periodic state always scatters in chaotic region and periodic attractors coexist with chaotic attractors in the dotted region. When $\sigma = 0.03259$, $k = -56.04$, if initial values are $(z_0, w_0, \theta_0, q_0) = (-0.19, 0.89, -0.76, -1.41)$, the phase track converges to a periodic attractor, while if initial values are $(z_0, w_0, \theta_0, q_0) = (-1.06, 2.35, -0.62, 0.75)$, the phase track converges to a chaotic attractor, coexisting attractors are shown in Figures 5(c) and 5(d), the periodic attractor is marked with red limit cycle, and the chaotic attractor is marked with blue. In addition, there are other types of multistability in the system at several combinations of parameters, such as coexistence of different stable

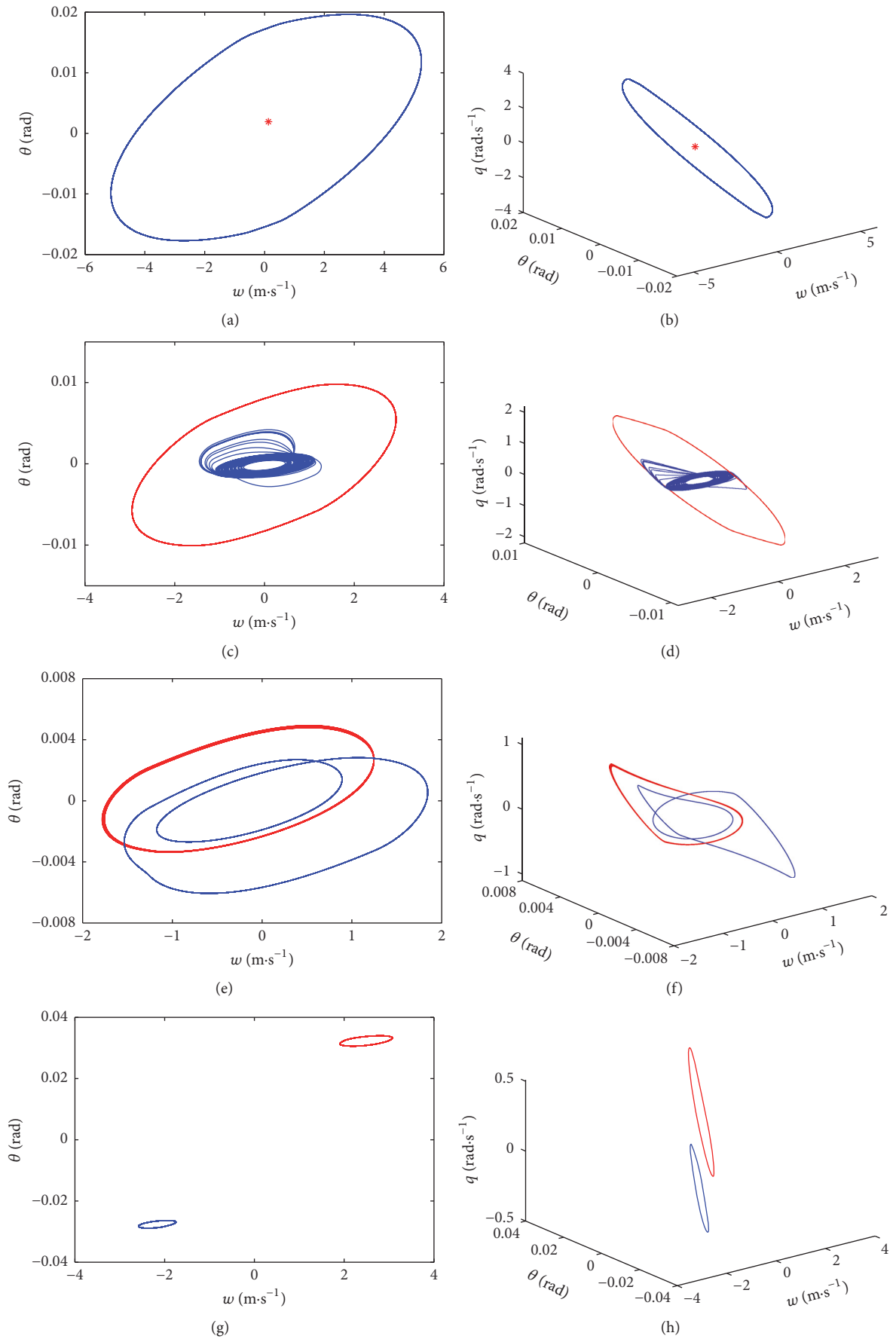

Figure 5: Continued.

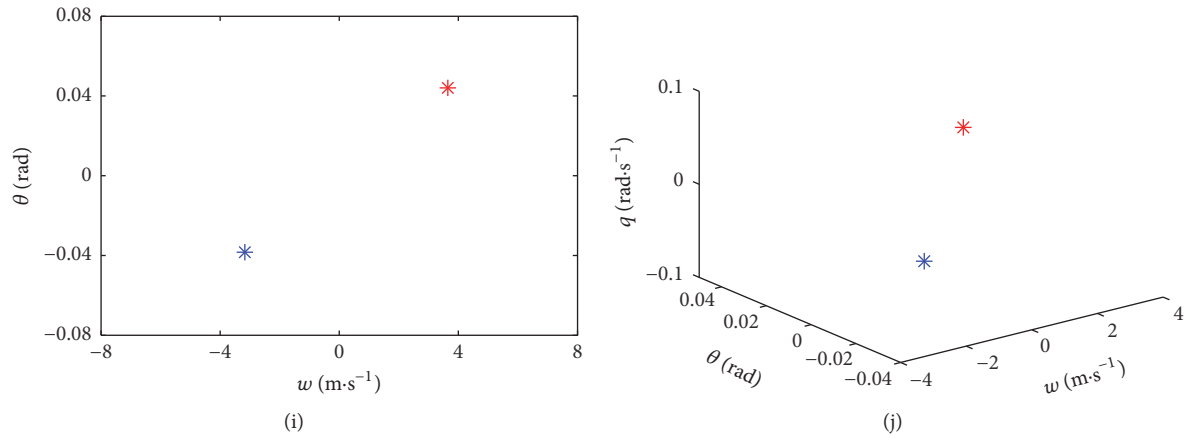

Figure 5: Projections of coexisting attractors on w-θ plane and w-θ-q space.

Table 2: Coexisting attractors at different combinations of parameters.

Type	Parameters	Initial conditions	Lyapunov exponent	Attractor dimensions
Coexistence of different stable equilibrium points	$\sigma = 0.02468$	$(0.84, -0.89, 0.10, -0.54)$	$(-5.55, -6.23, -86.48, -86.97)$	0
	$k = 9.011$	$(-1.42, 0.49, -0.18, -0.19)$	$(-8.29, -9.01, -63.41, -63.92)$	0
Coexistence of stable equilibrium point with periodic attractor	$\sigma = 0.02603$	$(0.32, -1.31, -0.43, 0.34)$	$(-11.88, -12.12, -28.46, -29.09)$	0
	$k = 5.901$	$(0.54, 1.83, -2.26, 0.86)$	$(0.014, -12.47, -17.83, -50.46)$	1
Coexistence of different 1-periodic cycles	$\sigma = 0.02805$	$(0.54, 1.83, -2.26, 0.86)$	$(-0.04, -11.65, -16.86, -65.67)$	1
	$k = 6.961$	$(-0.12, 1.49, 1.41, 1.42)$	$(0.01, -11.22, -15.95, -53.75)$	1
Coexistence of 1-periodic cycle with 2-periodic cycle	$\sigma = 0.03153$	$(1.44, -1.96, -0.20, -1.21)$	$(0.02, -2.14, -21.87, -75.92)$	1
	$k = -73.13$	$(0.30, -0.60, 0.49, 0.74)$	$(-0.02, -2.08, -21.15, -76.01)$	1
Coexistence of periodic attractor with chaotic attractor	$\sigma = 0.03238$	$(-1.09, 0.03, 0.55, 1.10)$	$(0.03, -21.16, -29.05, -29.90)$	1
	$k = -62.63$	$(-0.77, 0.37, -0.23, 1.12)$	$(2.31, -0.64, -85.20, -94.03)$	2.32

equilibrium points and coexistence of multiple limit cycles. When $\sigma = 0.03171$, $k = -71.432$, as shown in Figures 5(e) and 5(f), a red 1-periodic cycle coexists with a blue 2-periodic cycle. When $\sigma = 0.02805$, $k = 6.961$, as shown in Figures 5(g) and 5(h), two different kinds of 1-periodic cycles coexist. When $\sigma = 0.02468$, $k = 9.011$, as shown in Figures 5(i) and 5(j), two different kinds of stable equilibrium points coexist. If parameters are invariable, the coexisting attractors indicate behaviors of the system sensitive to initial conditions, the trajectory of supercavitating vehicle may probably approach two types of attractors when its initial depth, vertical velocity, pitch, and pitch rate are taken different values; namely, motion state of supercavitating vehicle is likely to be different.

(4) Within $\sigma \in [0.0198, 0.02956]$, $k \in [7.883, 17.79]$, the green stable dots scatter in the blue divergent region. When $k \in [-95, -85.78]$, red periodic dots scatter within the blue divergent region. In the interwoven regions, slight change in parameters can always lead to change in motion state of supercavitating vehicle; improper setting of initial conditions would make supercavitating vehicle capsize. Basins of attraction at stable equilibrium points and periodic dots are not stable persistently; they are likely to be divergent once beyond the boundary of basins of attraction.

4. Change in Robustness of Supercavitating Vehicle

It can be derived from above analysis that various coexisting attractors exist in the parameter regions marked with different colors in Figure 3, as shown in Table 2. As long as the coexisting attractors and their types are known, each attractor can be associated with all the initial conditions that make its trajectory approach this attractor; they constitute clustering region of the attractor, which is called the basins of attraction [14, 15]. So that the final state of the system is determined by the basins of attraction where initial conditions are located; when the initial conditions are near the boundary of the attraction basins, slight disturbance or change in parameters will lead to a completely different motion of the system. The initial conditions will bring high uncertainty in the final destination of the system as well, and complex behaviors [16, 17] often appear, which are likely to deviate from original expectation of designer and lead to unpredictable motion and thus pose a great threat to the engineering application. Therefore, it is essential to

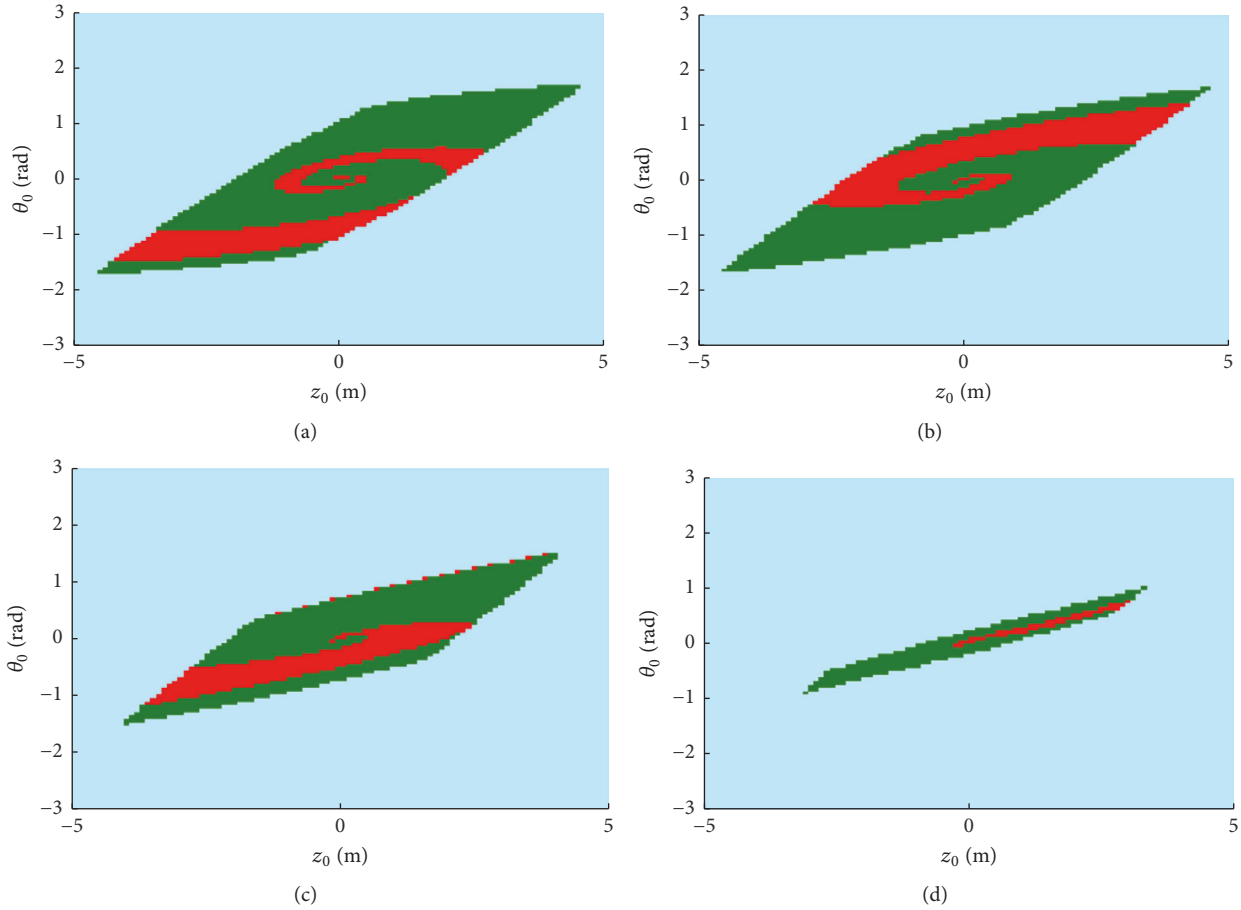

Figure 6: Basins of attraction: (a) $\sigma = 0.02468$, $k = 3.423$; (b) $\sigma = 0.02603$, $k = 5.901$; (c) $\sigma = 0.02721$, $k = 7.473$; (d) $\sigma = 0.02655$, $k = 9.369$.

understand such abnormal phenomena [18] thoroughly. For comprehensive analysis of a complex system, complexity of its attractors and its basins of attraction should be analyzed simultaneously. The study of basins of attraction is of high value in engineering application. Most engineering problems involve not only analysis of local stability and bifurcation under minor perturbation, but also scope of the attraction basins of steady solutions, that is, the area of attraction basins where steady solution is of same properties. With different launching conditions, the larger the area of attraction basins at steady state and periodic state, the stronger the robustness of supercavitating vehicle.

4.1. Basins of Attraction of Stable Equilibrium Point and Limit Cycle. Select various combinations of parameters from $\sigma \in [0.02620, 0.02973]$, $k \in [7.387, 14.325]$, namely, the region interwoven by stable, periodic, and divergent states; the sections of basins of attraction on z_0-θ_0 plane are shown in Figure 6 and basins of attraction are approximate to a parallelogram, when launching depth z_0 and launching pitch θ_0 are selected from green region in the figure; the lift of cavitator and fin is equal to the weight of supercavitating vehicle, which make supercavitating vehicle move stably under the parameters. When initial values are corresponding to the dots within red region, tail of supercavitating vehicle oscillates periodically moving into and out of the supercavity alternatively. When initial values are corresponding to the dots within blue region, too high values of initial conditions would lead to divergence of the system and the incapability of supercavitating vehicle to navigate. If any phase dot within basins of attraction of certain attractor is taken as initial condition, the system always converges to such attractor. In combinations of parameters, if cavitation number varies within a small range, the feedback control gain of fin deflection angle k decreases gradually; it can be proven by calculating the area of corresponding attraction basins that $S_{a1} > S_{b1} > S_{c1} > S_{d1}$, S_{a1}, S_{b1}, S_{c1}, and S_{d1} are areas of attraction basins in Figures 6(a), 6(b), 6(c), and 6(d), respectively. Therefore, provided that cavitation number varies within a small range, the area of attraction basins decreases with the feedback control gain of fin deflection angle k. With target to different initial launching conditions, the lower the value of k, the smaller the attraction basin of stable equilibrium point and periodic attractor and the weaker the robustness of the system, and hence supercavitating vehicle is more sensitive to external interferences and becomes unstable. In addition, when values of initial conditions are corresponding to the dots close to boundaries of the red region and the green region, slight interference can lead to the switching between stable motion and periodic

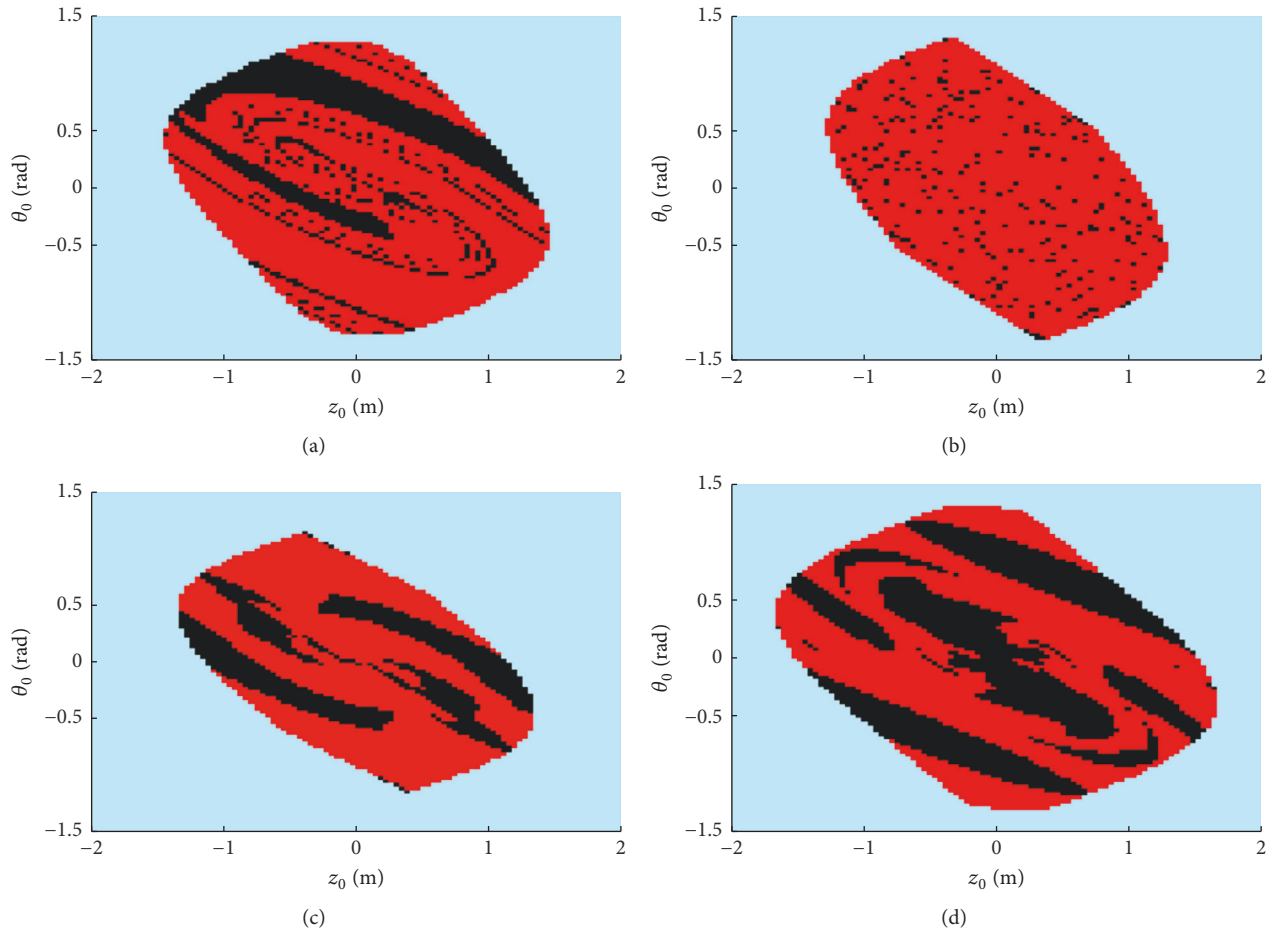

Figure 7: Basins of attraction: (a) $\sigma = 0.02838$, $k = -59.01$; (b) $\sigma = 0.03136$, $k = -67.44$; (c) $\sigma = 0.03238$, $k = -62.63$; (d) $\sigma = 0.03259$, $k = -56.04$.

oscillation of the vehicle. In practical engineering application, robustness of supercavitating vehicle can be improved by adjusting fin deflection angel of supercavitating vehicle and initial launching conditions.

4.2. Basins of Attraction of Limit Cycle and Chaotic Attractor. Select a few dots from $\sigma \in [0.02745, 0.03255]$, $k \in [-76.851, -52.573]$, namely, the region where periodic state interweaves with chaotic state; sections of their basins of attraction on z_0-θ_0 plane are shown in Figure 7, the red region represents the initial values falling into periodic trajectory, and supercavitating vehicle oscillates periodically. The black region represents the initial values which draw supercavitating vehicle to chaotic state eventually; supercavitating vehicle thus becomes unstable or even capsizes. The blue region represents the initial values which make the system divergent. In Figure 7, under different combinations of parameters, basins of attraction are almost same in shape, but with different sizes. There is a fractal boundary, in which slight change in initial conditions may probably trigger the transition of the system from stable periodic state to chaotic state and often lead to weaker robustness and even capsizing of supercavitating vehicle. In practical engineering application, it should be avoided to choose such variable combinations of parameters so as to improve robustness of the system.

4.3. Basins of Attraction of Stable Equilibrium Points. Select several dots from $\sigma \in [0.01980, 0.02956]$, $k \in [7.883, 17.794]$, namely, the region where stable state interweaves with divergent region. Sections of their basins of attraction on z_0-θ_0 plane are shown in Figure 8. If initial values z_0 and θ_0 are within green region, supercavity can be formed to enclose vehicle, and supercavitating vehicle moves stably. When the initial values are within the blue region rather than the green region, supercavitating vehicle becomes unstable. The bigger the basins of attraction, the stronger the robustness of the system. It can be seen from Figure 8 that if cavitation number varies within small range, the feedback control gain of fin deflection angle k decreases gradually, and the area of attraction basins of stable equilibrium points varies with combinations of parameters, $S_{a2} > S_{b2} > S_{c2} > S_{d2}$, where S_{a2}, S_{b2}, S_{c2}, and S_{d2} are area of attraction basins in Figures 8(a), 8(b), 8(c), and 8(d), respectively. The robustness decreases in such order. Therefore, within such scope, provided that cavitation number varies within a small range, the lower the value of k, the bigger the area of attraction basins and the stronger

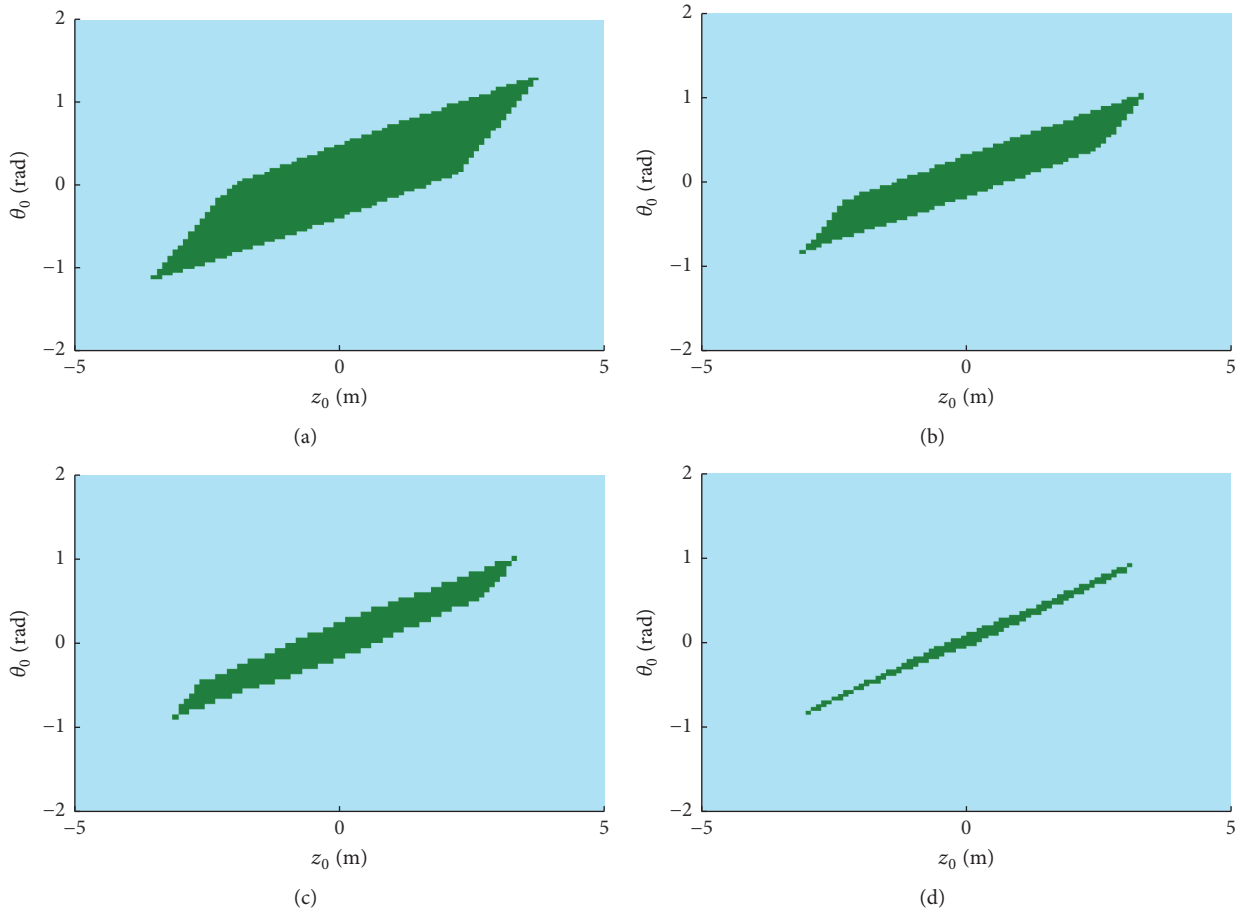

Figure 8: Basins of attraction: (a) $\sigma = 0.02788$, $k = 8.874$; (b) $\sigma = 0.02838$, $k = 9.369$; (c) $\sigma = 0.02754$, $k = 11.06$; (d) $\sigma = 0.02636$, $k = 10.04$.

the robustness; supercavitating vehicle is more liable to move stably. Figure 8 not only shows the range of initial conditions for stable motion of supercavitating vehicle but also reflects the relationship between the robustness and the parameters. In practical application, parameters with bigger basins of attraction and strong robustness should be selected to ensure stable motion of supercavitating vehicle.

4.4. Basins of Attraction of Limit Cycle. Select several dots from $k \in [-89.895, -85.786]$, namely, the region where periodic state interweaves with stable state. Sections of their basins of attraction on z_0-θ_0 plane are shown in Figure 9. If initial values z_0 and θ_0 are within the red region, periodic oscillation occurs due to collision between the tail of supercavitating vehicle and the supercavity from time to time; supercavitating vehicle is in periodic oscillation. When the initial values are corresponding to the dots within the blue region, the system is divergent and supercavitating vehicle capsizes. It can be seen from Figure 9 that provided that cavitation number varies within small range, the area of attraction basins decreases with value of k gradually. Therefore, value of k has significant effect on robustness of supercavitating vehicle, which becomes weaker with increase of k.

4.5. Basins of Attraction of Other Types. It can be found from analysis of dynamic distribution diagram that coexistence of stable equilibrium point with limit cycle and coexistence of limit cycle with chaotic attractor are universal phenomena of multistability. In addition, there are other types of multistability at individual parameters in the system, such as coexistence of 1-periodic cycle with 2-periodic cycle, coexistence of two types of 1-periodic cycles, and coexistence of two types of stable equilibrium points. For the coexistence of 1-periodic cycle with 2-periodic cycle, sections of basins of attraction on z_0-θ_0 plane are shown in Figures 10(a) and 10(b), respectively. The red region represents the initial values which make supercavitating vehicle approach the 1-periodic trajectory eventually. The dark blue region represents the initial values which make vehicle approach 2-periodic trajectory eventually. The light blue region represents divergence of the system. Therefore, different initial launching conditions may probably result in different periods of motion. Basin of attraction for coexistence of two types of 1-periodic cycles is shown in Figure 10(c); the red region and the dark blue region represent the initial values which make supercavitating vehicle fall into different periods of oscillation eventually. With such combinations of parameters, supercavitating vehicle may display different periodic microoscillation under different

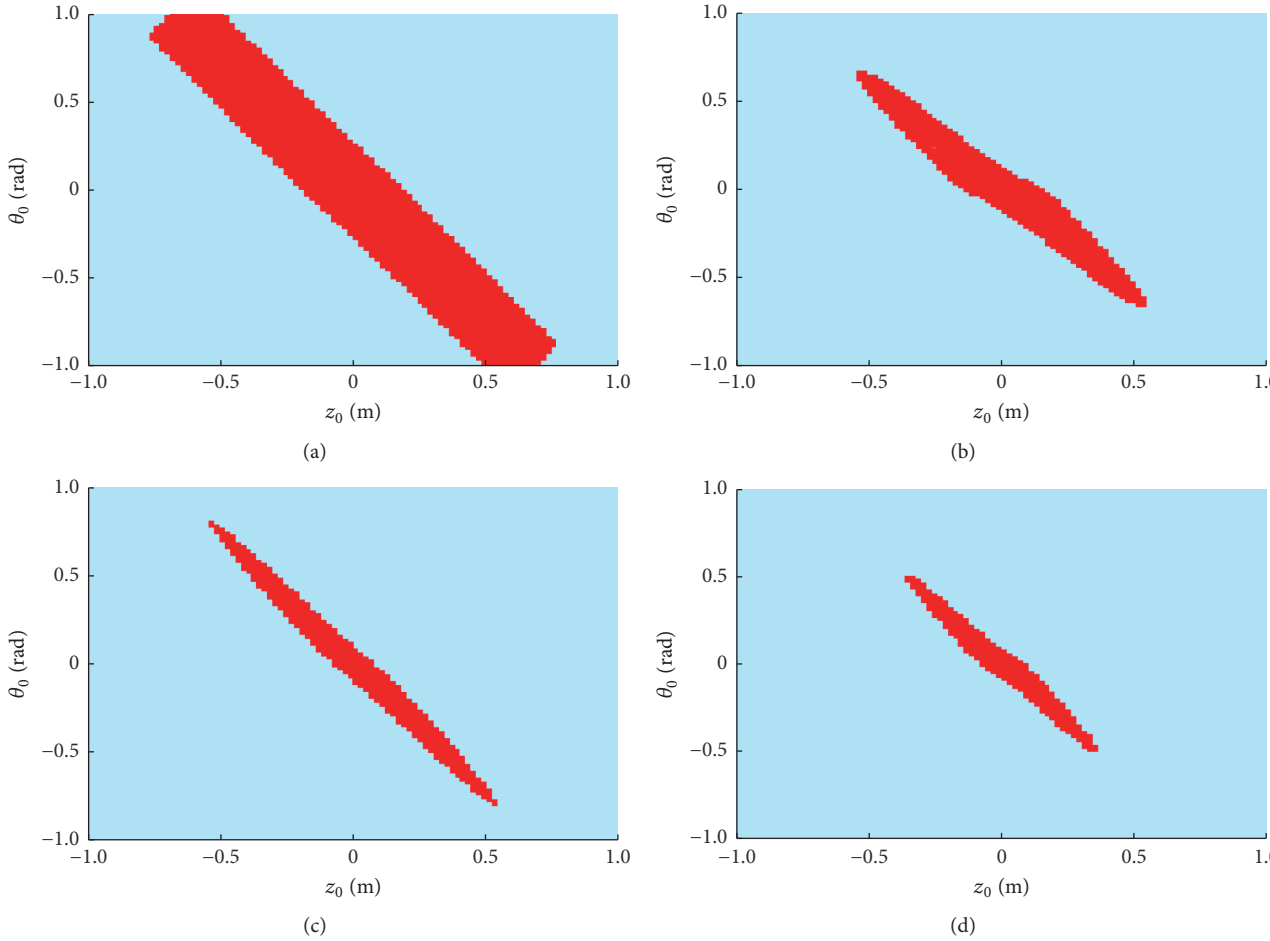

Figure 9: Basins of attraction: (a) $\sigma = 0.02434$, $k = -87.83$; (b) $\sigma = 0.03040$, $k = -91.93$; (c) $\sigma = 0.02805$, $k = -90.9$; (d) $\sigma = 0.03428$, $k = -89.88$.

initial conditions. Basin of attraction for coexistence of two types of stable equilibrium points is shown in Figure 10(d); when initial values correspond with the red region and the dark blue region, the motion of supercavitating vehicle will approach two different types of stable equilibrium points. Supercavitating vehicle can navigate stably if initial values are within the basin of attraction. The system is divergent and the vehicle capsizes once initial values are beyond the boundary of the basin of attraction.

5. Conclusion

In this paper, general characteristics of dynamic behaviors of supercavitating vehicle are studied with dynamic distribution diagram based on a 4-dimensional dynamic model, coexistence of various attractors is confirmed herein, and the relation between the robustness of supercavitating vehicle and the parameters of system and initial values is obtained though multistability analysis. Following conclusions can be drawn:

(1) In the system of supercavitating vehicle, select any two parameters as variable parameters, through dynamic distribution diagram, the relationship between dynamic behaviors and variable parameters can be obtained. And the regions of parameters where coexisting attractors are likely to be found are disclosed, providing the basis for setting parameters for stable motion.

(2) Basins of attraction vary with parameters of the system, some attractors will die, and new attractors will be generated. Basins of attraction can be used to determine the range of initial conditions for stable motion of supercavitating vehicle, and unstable motion can be prevented by adjusting initial values of launch.

(3) Generally, supercavitating vehicle has three stable states, including stable, periodic, and chaotic states. Under appropriate combinations of parameters, there are various motions of multistability, such as coexistence of two types of stable equilibrium points, coexistence of a stable equilibrium point with a limit cycle, coexistence of a limit cycle with chaotic attractor, and coexistence of multiple limit cycles.

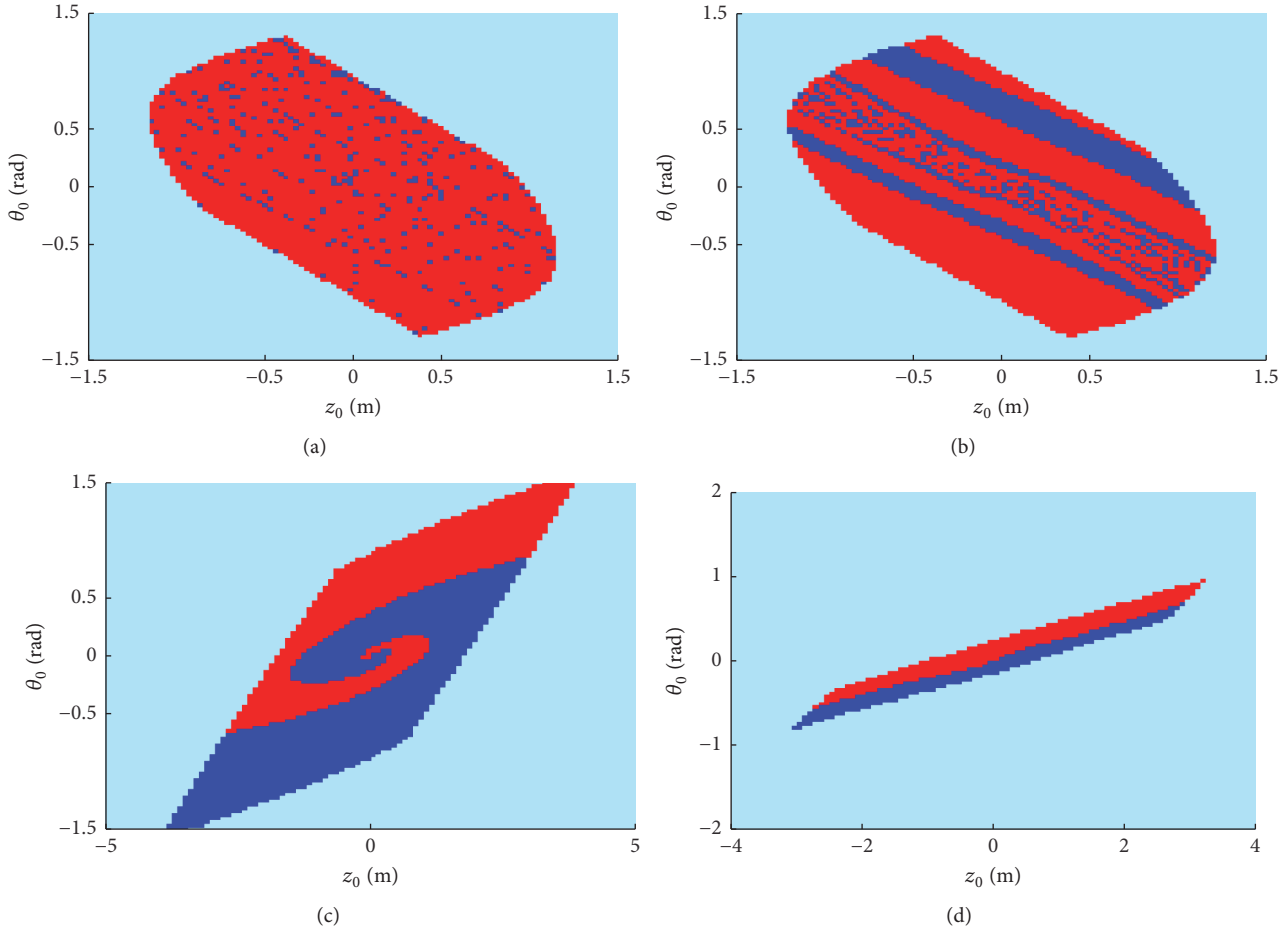

Figure 10: Basins of attraction (a) $\sigma = 0.03171$, $k = -71.43$; (b) $\sigma = 0.03187$, $k = -70.94$; (c) $\sigma = 0.02805$, $k = 6.961$; (d) $\sigma = 0.02464$, $k = 9.011$.

When parameters are fixed, supercavitating vehicle may display different states of motion under different initial values.

(4) Provided that cavitation number varies within a small range, robustness of the system becomes weaker with the increase of feedback control gain of fin deflection angle k; size of basins of attraction becomes smaller and robustness of the system becomes weaker. Systematic parameters with greater basins of attraction can be selected to lessen sensitivity to external interference and improve robustness of supercavitating vehicle.

Conflicts of Interest

The authors declare that there are no conflicts of interest regarding the publication of this paper.

Acknowledgments

This work is supported by the National Natural Science Foundation of China (Grant nos. 11402116 and 11472163) and the Fundamental Research Funds for the Central Universities (Grant no. 30910612203).

References

[1] A. Ducoin, B. Huang, and Y. L. Young, "Numerical modeling of unsteady cavitating flows around a stationary hydrofoil," *International Journal of Rotating Machinery*, vol. 2012, Article ID 215678, 17 pages, 2012.

[2] B. Vanek, J. Bokor, G. J. Balas, and R. E. A. Arndt, "Longitudinal motion control of a high-speed supercavitation vehicle," *Journal of Vibration and Control*, vol. 13, no. 2, pp. 159–184, 2007.

[3] Q.-T. Li, Y.-S. He, L.-P. Xue, and Y.-Q. Yang, "A numerical simulation of pitching motion of the ventilated supercaviting vehicle around its nose," *Chinese Journal of Hydrodynamics. A*, vol. 26, no. 6, pp. 689–696, 2011.

[4] J. Dzielski and A. Kurdila, "A benchmark control problem for supercavitating vehicles and an initial investigation of solutions," *Journal of Vibration and Control*, vol. 9, no. 7, pp. 791–804, 2003.

[5] M. A. Hassouneh, V. Nguyen, B. Balachandran, and E. H. Abed, "Stability analysis and control of supercavitating vehicles with

advection delay," *Journal of Computational and Nonlinear Dynamics*, vol. 8, no. 2, Article ID 021003, 10 pages, 2013.

[6] B. Vanek, J. Bokor, and G. Balas, "Theoretical aspects of high-speed supercavitation vehicle control," *American Control Conference*, vol. 6, no. 3, pp. 1–4, 2006.

[7] G. Lin, B. Balachandran, and E. H. Abed, "Nonlinear dynamics and bifurcations of a supercavitating vehicle," *IEEE Journal of Oceanic Engineering*, vol. 32, no. 4, pp. 753–761, 2007.

[8] G. Lin, B. Balachandran, and E. H. Abed, "Bifurcation behavior of a supercavitating vehicle," in *Proceedings of the ASME International Mechanical Engineering Congress and Exposition*, pp. 293–300, Chicago, Ill, USA, November 2006.

[9] G. J. Lin, B. Balachandran, and E. H. Abed, "Dynamics and control of supercavitating vehicles," *Journal of Dynamic Systems, Measurement, and Control*, vol. 130, no. 2, Article ID 021003, pp. 281–287, 2008.

[10] B. Vanek and G. Balas, "Control of high-speed underwater vehicles," *Control of Uncertain Systems: Modeling, Approximation and Design*, no. 329, pp. 25–44, 2006.

[11] A. Goel, *Robust control of supercavitating vehicles in the presence of dynamic and uncertain cavity [Doctor's thesis]*, University of Florida, Gainesville, Fla, USA, 2005.

[12] X. H. Zhao, Y. Sun, Z. K. Qi, and M. Y. Han, "Catastrophe characteristics and control of pitching supercavitating vehicles at fixed depths," *Ocean Engineering*, vol. 112, pp. 185–194, 2016.

[13] M. L. Wang and G. L. Zhao, "Robust controller design for supercavitating vehicles based on BTT maneuvering strategy," in *Proceedings of the International Conference on Mechatronics & Automation*, pp. 227–231, 2007.

[14] G. A. Leonov and N. V. Kuznetsov, "Hidden attractors in dynamical systems: from hidden oscillations in hilbert-kolmogorov, Aizerman, and Kalman problems to hidden chaotic attractor in chua circuits," *International Journal of Bifurcation and Chaos*, vol. 23, no. 1, Article ID 1330002, 2013.

[15] M. Chen, M. Li, Q. Yu, B. Bao, Q. Xu, and J. Wang, "Dynamics of self-excited attractors and hidden attractors in generalized memristor-based Chua's circuit," *Nonlinear Dynamics*, vol. 81, no. 1-2, pp. 215–226, 2015.

[16] J. C. A. de Bruin, A. Doris, N. van de Wouw, W. P. M. H. Heemels, and H. Nijmeijer, "Control of mechanical motion systems with non-collocation of actuation and friction: a Popov criterion approach for input-to-state stability and set-valued nonlinearities," *Automatica*, vol. 45, no. 2, pp. 405–415, 2009.

[17] M. A. Kiseleva, N. V. Kuznetsov, G. A. Leonov, and P. Neittaanmäki, "Drilling systems failures and hidden oscillations," in *Proceedings of the IEEE 4th International Conference on Nonlinear Science and Complexity (NSC '12)*, pp. 109–112, IEEE, Budapest, Hungary, August 2012.

[18] G. A. Leonov, N. V. Kuznetsov, O. A. Kuznetsova, S. M. Seledzhi, and V. I. Vagaitsev, "Hidden oscillations in dynamical systems," *WSEAS Transactions on Systems and Control*, vol. 6, no. 2, pp. 54–67, 2011.

[19] T. Lauvdal, R. M. Murray, and T. I. Fossen, "Stabilization of integrator chains in the presence of magnitude and rate saturations; a gain scheduling approach," in *Proceedings of the 36th IEEE Conference on Decision and Control*, pp. 4004–4005, December 1997.